Understanding and Expanding the Prospects for Electrosynthesis with Liquid Metal Electrodes

Henry Wu,[1‡] Joshua P. Hazelnis,[1‡] and Stephen Maldonado[1,2]*

1. *Department of Chemistry, University of Michigan, Ann Arbor, Michigan 48109-1055, USA*

2. *Program in Applied Physics, University of Michigan, Ann Arbor, Michigan 48109-1055, USA*

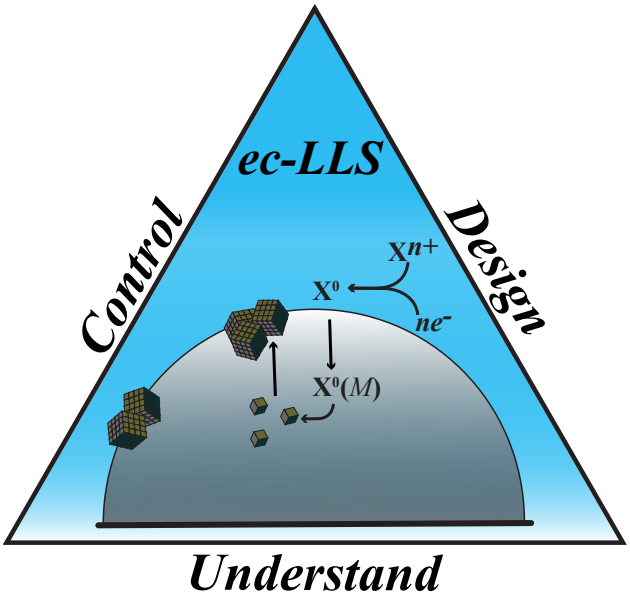

Conspectus.

This account describes and summarizes the latest work from our lab on developing and maturing strategies based on low temperature liquid metals as reaction environments for materials synthesis. The electrochemical liquid-liquid-solid (ec-LLS) crystal growth concept is a hybrid method that combines electrodeposition and melt crystal growth. Using liquid metals as both electrodes and solvents for the purpose of producing inorganic crystals and materials, a simple and environmentally-friendly process is possible. The impetus is to address the key deficiency in the inorganic crystalline materials that are the basis of modern optoelectronics and renewable energy capture/conversion systems. Specifically, existing methods for synthesizing crystalline inorganic materials for these purposes are largely energy and resource intensive, with substantial impact on the environment when scaled. A long term goal of our work with ec-LLS is to realize a materials synthetic process that is matured without requiring intensive resources or negatively impacting the environment. To this end, the factors that both limit and govern ec-LLS processes must be identified and understood. To date, questions regarding the factors that affect crystal nucleation & growth, form factors, and overall composition remain.

Previous work established concretely ec-LLS as a versatile method for synthesizing and producing crystalline semiconductors at low temperatures as either particles, nanowires, or microwires. Subsequent experiments have focused on two tiers. First, the microscopic details of the liquid metal and its interfaces that dictate materials synthesis and crystal growth must be identified. Second, strategies that widen the attainable material form factors to facilitate device architectures must be realized. Hence, this account describes results aimed at answering three questions: (*1*) What are the consequences of reaching supersaturation by an electrochemical rather than a thermal driving force for crystal growth in ec-LLS? (*2*) Can the location of nucleation and subsequent crystal growth be controlled? (*3*) Does the atomic structure of the liquid metal affect product formation in ec-LLS? The science described herein illustrates the value of in-situ methods spanning transmission electron microscopy, X-ray diffraction, and X-ray reflectance for revealing the role that liquid metal composition and structure can play in ec-LLS. Additionally, we summarize work that shows for the first time that it is possible to produce both single-crystalline epitaxial films and complex intermetallic compounds through ec-LLS by tuning the cell design, electrochemical excitation waveform, and composition of the liquid metal electrodes.

The cumulative findings described here substantially enrich our understanding of the ec-LLS concept while simultaneously motivate further questions moving forward. Is it possible to attain complete control over the crystalline quality and composition of ec-LLS products? Can the materials produced by ec-LLS provide tailored functional properties for targeted applications? Can the ec-LLS strategy be further refined to allow material synthesis and deposition at precise locations with deterministically chosen form factors? What synthetic pathways are accessible when even more sophisticated electrochemical waveforms and cell designs are used? Our hope is that this account will spur additional researchers to help answer such questions.

⸸ These authors contributed equally

* To whom correspondence should be addressed.
Phone: +1-734-647-4750. e-mail: smald@umich.edu; Home Page: http://www.umich.edu/~mgroup/

Key References.

- Cheek, Q.; Fahrenkrug, E.; Hlynchuk, S.; Alsem, D. H.; Salmon, N. J.; Maldonado, S., In Situ Transmission Electron Microscopy Measurements of Ge Nanowire Synthesis with Liquid Metal Nanodroplets in Water. *ACS Nano* **2020,** *14*, 2869-2879.[1] *In-situ liquid TEM measurements are performed on aqueous suspensions of liquid metal nanodroplets during Ge nanowire ec-LLS.*

- Demuth, J.; Fahrenkrug, E.; Ma, L.; Shodiya, T.; Deitz, J. I.; Grassman, T. J.; Maldonado, S., Electrochemical Liquid Phase Epitaxy (ec-LPE): A New Methodology for the Synthesis of Crystalline Group IV Semiconductor Epifilms. *Journal of the American Chemical Society* **2017,** *139* (20), 6960-6968.[2] *The first electrodeposition of macroscale single-crystalline semiconductor epifilms by the method of ec-LPE is demonstrated.*

- Downes, N.; DeMuth, J.; Waelder, J.; Cheek, Q. B.; Bartels, H.; Maldonado, S., Si Electrochemical Liquid Phase Epitaxy: Low-Temperature Growth of Hyperdoped Epitaxial Si Films. *Chemistry of Materials* **2022**, *34*, 10861-10872.[3]*Room temperature electrodeposition of single crystalline Si epitaxial films using ec-LPE with a pulsed waveform is highlighted.*

- Pattadar, D.; Cheek, Q.; Sartori, A.; Zhao, Y.; Giri, R. P.; Murphy, B.; Magnussen, O.; Maldonado, S., Evidence for Facilitated Surface Transport during Ge Crystal Growth by Indium in Liquid Hg–In Alloys at Room Temperature. *Crystal Growth & Design* **2021,** *21* (3), 1645-1656.[4] *The first data are reported for Hg-In liquids during Ge electrodeposition that illustrate surface enrichment of Hg at the liquid metal/liquid electrolyte interface and In at the liquid metal/solid crystal interface*

Background and Context

Liquid metals were essential to the discovery and the synthesis of many historically important crystalline inorganic materials. At the onset of the semiconductor age, high temperature liquid metals were crucial in both the fundamental understanding of crystal growth[5] and the practical production of high quality materials for optoelectronic devices.[6] Interest in liquid metals as platforms for materials science continues to this day.[7-11] A vibrant new direction focuses on metals and metal alloys that are molten at or near room temperature.[12] Room temperature liquid metals allow the syntheses of several previously unimagined material phases and compositions.[13-17] The preparation of ultra-thin (i.e. two dimensional) oxides is now possible because the composition of a surface oxide on a liquid metal mixture can be selectively tuned.[14] Similarly, the facile synthesis of two-dimensional metal films (e.g. gallanene)[18,19] is known.[14,20]

In a previous account,[21] we described a new hybrid strategy for synthesis of inorganic semiconductors centered on the virtues of liquid metals. The electrochemical liquid-liquid-solid (ec-LLS) concept utilizes liquid metals as chemical solvents and as electronic current collectors. The use of a liquid metal as an electrode during electrodeposition affords the possibility of obtaining a crystalline form of the electrodeposit (Figure 1a). An appeal of ec-LLS is that the common three electrode cell design in electrodeposition becomes a highly versatile melt crystal growth reaction vessel (Figure 1b).

The ec-LLS method has several tangible advantages. Ec-LLS is natively simple to execute since heating/cooling and vacuum equipment are not required. Ec-LLS is not specific to just the common liquid metals in electrochemistry (i.e. Hg), having been performed with other pure liquid metals and molten alloys.[4,22-24] Ec-LLS is agnostic towards electrolyte type, i.e. both molecular and ionic electrolyte solvents are suitable.[25,26] Ec-LLS can be performed with large or minute volumes of liquid metals.[27,28]

Still, ec-LLS is deceptively complex to optimize. Beyond pure engineering challenges, translating ec-LLS to practical scales for target applications requires a more complete understanding of what materials are (and are not) possible to synthesize and what aspects are most relevant. There are several critical and fundamental knowledge gaps in how to think about liquid metal solvent electrodes. In general, the atomic structure and depth-dependent composition are significantly more nuanced for liquid metal solvents than for molecular liquids.[29,30] More specifically, a complete picture of liquid metals in contact with liquid electrolytes with and without an applied bias is lacking at the atomic scale.

Separately, crystal growth by an electrochemical (rather than a thermal) gradient is fundamentally different than any traditional type of melt crystal growth. Even for well studied materials, the consequences of this difference are difficult to predict.

This review summarizes and contextualizes work from our group focused on filling in these knowledge gaps. Unlike the preceding account which focused on studies that demonstrated or verified the ec-LLS idea, the work contextualized here focuses on either defining how crystalline solids form in a liquid metal electrode, refining the ec-LLS concept towards realizing more advanced material targets, or both. In total, the observations, inferences, and conclusions of the summarized research address three pressing questions (Figure 1b insets): (*1*) How is crystal growth impacted when supersaturation in a liquid metal solution is attained by an electrochemical bias rather than temperature drop? (*2*) Can the location of nucleation and subsequent crystal growth be controlled? (*3*) Does the atomic structure of the liquid metal affect product formation in ec-LLS?

Supersaturation by an Electrochemical Driving Force

A consistent observation in our lab was that crystals in ec-LLS did not appear instantaneously. We never observed an initial deposition of amorphous/disordered solute in any ec-LLS configuration, ruling out this possibility.[25,31-33] Instead, we suspected that an appreciable amount of electrodeposited solute accumulated within the liquid metal electrodes prior to eventual crystal growth.

Initial measurements were performed with X-ray diffraction on eutectic gallium indium (*e*-GaIn) microdroplets of precisely defined volumes. The premise was that diffraction from (111) planes would serve as a marker for the formation of Ge crystals in ec-LLS by the electroreduction of dissolved GeO_2.[34] Linear correlations of the X-ray diffraction signal intensity vs time (t) were consistently observed at several different temperatures, but none of the collected data sets had intercepts at t=0. Instead, extrapolation of these linear data sets indicated a delay in the first appearance of Ge crystals between 15 and 45 s. Complementary 1D models of diffusion and nucleation/crystal growth in the liquid metal microdroplets indicated that these delay times might be better understood as induction times. These data implied that driving forces for nucleation and crystal growth of 14 kJ mol^{-1} were attained at first detection of crystals. These driving forces corresponded supersaturation levels of Ge $>10^2$ (i.e. concentrations 100x larger than the equilibrium solubility limit) in *e*-GaIn during ec-LLS. These large driving force and supersaturations were surprising, implying two important points. First, the activation barrier for nucleation in at least some low temperature ec-LLS processes is much higher than k_BT. Second, liquid metal electrodes in ec-LLS are, with respect to solute solubility, solutions far

from equilibrium. The first point was consistent with reports suggesting that liquid metals that are poorer solvents for Ge require high supersaturations to grow Ge crystals.[35] The equilibrium solubility for Ge in *e*-GaIn near room temperature is much lower in comparison to the solubility of Ge in Au (~0.2 mol L^{-1}), [36,37] Still, our data also suggested the activation barrier for nucleation depended on the size of the microdroplet (*vide infra*). The fact that the liquid metal droplets were in contact with multiple surfaces introduced uncertainty in interpretation of the activation barriers for nucleation. The second point provided some context as to why defects are consistently observed in crystals prepared by ec-LLS. Still, the sensitivity of X-ray diffraction further introduced uncertainty with regards to the precise induction times and the actual supersaturation levels.

To provide further clarity, we pursued an alternative method for in-situ analysis, liquid cell transmission electron microscopy (TEM).[1] This technique[38] allows direct visualization of nucleation and crystal growth in liquid solvents. An added benefit is the possibility that the electron beam used for imaging can drive electrochemical processes.[39] In the context of ec-LLS, this latter aspect afforded biasing isolated, suspended liquid metal droplets to drive electrodeposition without nucleation at a solid interface (Figure 2a). When the electrolyte contains the appropriate ec-LLS precursor, the incident electron beam can stimulate electroreduction. Figure 2b shows representative frames from different times of one such experiment for a Ge ec-LLS event at room temperature that produced a nanowire from a Ga nanodroplet. The temporal resolution was limited by the quality of the digital detector. State-of-the-art detectors are capable of significantly faster frame rates. Nevertheless, precise nanowire growth rates were easily determined (Figure 2c). More interestingly, quantitative analysis of the volume of the liquid metal prior to, during, and after the emergence of the Ge crystal was possible, assuming symmetry in three-dimensional space from the projected two-dimensional images. The inferred volume at each frame informed on the time-dependent loading of Ge in liquid Ga nanodroplets (Figure 2e). Extremely high atomic fractions (>50%) were consistently observed for both liquid Ga and In droplets. For context, the binary phase diagram for Ge and Ga is shown in Figure 2e. At room temperature, the equilibrium solubility of Ge in Ga is vanishingly small. But under an applied bias, Ga-Ge liquid mixtures can reach supersaturations that are equivalent to a state supercooled by 775 degrees K! Supercooling stabilized by an electrochemical bias has subsequently and independently been verified.[40] Thus, these experiments indicated that while ec-LLS experiments have many similarities with traditional melt crystal growth approaches like vapor-liquid-solid methods, ec-LLS also affords both unique and potentially tunable conditions for materials synthesis.

Controlling the Location of Nucleation and Crystal Growth

The aforementioned works also provided insight on controlling where nucleation and crystal growth occurs with liquid metal electrodes. Figures 3a and 3b highlight a hypothesis that we tested initially with liquid metal microdoplets.[34] Using narrow, lithographically patterned microwells, we assessed where Ge crystals grew with liquid metal microdroplet electrodes possessing different thicknesses. We posited that there is a critical distance between the top liquid/liquid and bottom liquid/solid interfaces that defines where solute will crystallize. Specifically, if the liquid metal was too thick, the solute would accumulate within the bulk of the liquid metal and nucleate at that location (buoyancy of the resultant Ge crystals in *e*-GaIn would result in accumulation at the top interface). Conversely, if the liquid metal was sufficiently thin, the probability would be high for the solute to reach the bottom liquid/solid interface and preferentially nucleate there. Crystal growth then pushes the liquid metal out of the microwell.

Representative results from these experiments are shown in Figures 3c,d. At a temperature just above the melting point, liquid *e*-GaIn droplets thicker than 20 μm showed numerous Ge crystallites at the top interface. Conversely, liquid *e*-GaIn droplets thinner than 10 μm supported the electrodeposition of a crystalline Ge microwire. Nucleation occurred exclusively at the bottom interface and crystal growth continued specifically at the liquid metal/solid Ge interface. No solid material nucleated or accumulated on the side walls of the photoresist. This general feature was observed at other temperatures, except the apparent thickness threshold for observing 'clean' microwire growth increased at higher temperatures.

We inferred that the thickness threshold for ensuring that ec-LLS resulted in heterogeneous nucleation at the bottom interface was not unique to the microwell platform. That is, if a sufficiently thin but *wide* liquid metal electrode were used for ec-LLS, the electrodeposited material would grow exclusively as a *film* at the bottom interface with the substrate. Figure 3e illustrates the basic concept, with Figure 3f illustrating a microscopic view that relates the diffusion pathlength of the solute and the liquid metal thickness. Although fabricating arbitrarily wide wells in photoresist is trivial, we empirically found that patterned features with aspect ratios greater than ~2 (i.e. width divided by thickness) could not be reliably wet by and filled with liquid metals. Accordingly, alternate strategies were necessary to test this hypothesis.

Liquid metals that wet a substrate can be mechanically spread. *e*-GaIn seemingly wets several types of solid surfaces. However, that wettability is dictated by the native oxide of *e*-GaIn. The bare surface of liquid metals does not wet most non-metallic materials. Ec-LLS requires cathodic potentials

that remove surface oxide. This point, in conjunction with the electrocapillarity of liquid metals,[41] compromises liquid metal films in ec-LLS. That is, thin liquid metal films break up into discrete liquid metal macro-, micro-, and nanodroplets when negatively biased. This observation was particularly true for liquid *e*-GaIn films spread over single-crystalline semiconductor substrates.

Accordingly, we invented a new type of electrodeposition cell. Figure 3g summarizes the key elements. In this compression cell, a semiconductor wafer substrate is patterned with an insulating material that defines a liquid metal reservoir with a large area but shallow depth. The depth is defined by the insulator thickness but intentionally kept ≤ 10 μm. This cavity is filled with liquid metal and the substrate is then sandwiched between a support platform and a porous membrane. The porous membrane constrains the liquid metal to prevent breaking apart but preserves contact between the liquid metal and liquid electrolyte.

The cell in Figure 3g allows ec-LLS growth where nucleation occurs solely at the liquid metal/substrate interface. Provided the substrate is lattice-matched to the intended solute crystal, the result is electrodeposition of *epitaxial* films (i.e. epifilms). Epitaxy is highly desirable in semiconductor film deposition and is generally unthinkable for covalent semiconductor electrodeposition, particularly at low temperatures. We dubbed ec-LLS experiments where macroscopic epitaxial films are produced electrochemical liquid phase epitaxy (ec-LPE).

The ec-LPE concept was first realized with the electrodeposition of Ge epifilms.[2] Figure 4a summarizes electrochemical data obtained when thin liquid *e*-GaIn films were used for Ge ec-LLS. The inset highlights the simplicity of the electrochemical waveform, i.e. a constant negative bias was applied for several hours. Disassembly of the cell and removal of the liquid metal revealed a large-area Ge film strongly adhered to the wafer substrate (Figure 4b). The film width was dictated by the dimensions of the ec-LPE cell. A separate 'large'-area ec-LPE cell afforded the electrodeposition of Ge epifilms spanning a 6" wafer substrate. Figure 4c illustrates the uniformity of these Ge epifilms. Irrespective of the width, the film thickness was dictated by the total time and charge passed as well as the electrodeposition temperature. The continuity between the substrate and epifilm crystallinity was apparent in both dark-field STEM and in selected area diffraction patterns (Figure 4d-f). Closer inspection of the interface between the substrate and the electrodeposited epifilm illustrated one of the most astounding aspects of ec-LPE. There was no evidence of an intervening oxide layer. The prevailing wisdom in semiconductor material synthesis and deposition is that the employed ec-LPE conditions are *anathema* to obtaining atomically clean interfaces. Yet, even though the

electrodeposition was performed *with water* in a cell operated in *lab ambient* at nearly *room temperature*, epifilms were readily obtained.

An obvious target for low-temperature ec-LPE are Si epifilms. Low temperature growth of crystalline Si is a major step towards non-toxic, inexpensive, environmentally responsible, and efficient photovoltaics.[42] Despite the early identification of Si ec-LLS processes for crystalline particles[43] and for crystalline nanowires,[27] Si ec-LPE proved significantly more challenging than Ge. In addition to requiring non-aqueous solvents and slightly elevated temperatures, the $SiCl_4$ precursor is prone to extensive side reactions at negative applied bias.[44] This aspect prevented growth of Si epifilms with thicknesses much beyond 10 nm.

We used a pulsed electrodeposition waveform (Figure 4g) that prevents accumulation of deleterious side products.[3] Macroscopic Si epifilms with micron thicknesses were then readily obtained (Figures 4h,i). The collected microscopic and diffraction data indicated the crystal structure of the electrodeposited films was a direct extension of the underlying substrate without any obvious sign of intervening oxide layer (Figure 4j-l). A consistent feature in both Si and Ge epifilms has been extensive incorporation of Ga. The resultant hyperdoping specifically for this metal suggests more understanding is needed to prevent metal incorporation at the crystal growth interface.

Influence of the Local Atomic Structure and Composition of Liquid Metal Electrodes

Additional methods are necessary to interrogate the microscopic details of liquid metal interfaces. Electron scatter by the liquid electrolyte limits the attainable imaging resolution in *in-situ* TEM. X-ray reflectivity (XRR) stands alone in elucidating interface structure with atomic resolution (along the surface normal).[29] XRR requires high intensity and photon energies to access buried liquid-liquid interfaces but is the first technique to unambiguously identify one of the most unusual aspects of liquid metal interfaces – atomic layering. Specifically, a characteristic maximum is observed in the normalized XRR signal that corresponds to a quasi-Bragg peak arising from atomic layering in the near-surface region of the liquid metal. This peculiar atomic structure occurs because the stark electronic differences between the liquid metal and the surrounding medium are so great that the entropic penalty of organization of the liquid metal atoms is overcome by the free energy gain of minimizing interaction between the liquid metal atoms and the outside media.

Figure 5a illustrates the data obtained for Hg immersed in aqueous electrolyte containing 0.1 M $Na_2B_4O_7$. The experimental measurements were well fit with a model consisting of Hg atoms

arranged with order that dissipated moving perpendicular from the surface plane towards the bulk (Figure 5a inset). Extensive XRR measurements were collected to compare Hg immersed in this electrolyte and NaF(*aq*).[45] The latter system is the most well-studied liquid metal/water interface,[41] with Hg exhibiting atomic structure nearly identical to the Hg/vacuum interface.[17] Since the XRR data for Hg/$Na_2B_4O_7$(*aq*) contacts were statistically indistinguishable from data for Hg/NaF(*aq*) junctions, the former interface was concluded to have essentially the same pristine character and structure as the latter.

Those data were contrasted with measurements performed with Hg-In alloys. Hg-In alloys are interesting because In can range from 0 to ~70 at.% while still being a liquid at room temperature. The XRR data for $Hg_{0.3}In_{0.7}$ are shown in Figure 5b. The characteristic layering peak could again be observed, although with greater intensity than for pure Hg. More interestingly, the data could only be fit with a model where the outermost atomic layer was composed almost entirely of Hg. This observation was consistent with ideal mixture behavior, where the component with the lower surface energy has a higher fractional composition on the surface than in the bulk.[46] Thus, these XRR data were the first to illustrate enriched atomic structure of a liquid metal alloy/liquid electrolyte interface.

This surface segregation of Hg confirmed that the *local* liquid metal structure and composition were malleable. We posited that the interfacial structure would be quite different in contact with Ge crystals since molten In more readily wets Ge wafers than Hg.[47] The surface tension for In/Ge is 0.58 N m^{-1} at $T = 25$ °C while for Hg/Ge it is >1.1 N m^{-1}.[4] In this case, In should *accumulate* at this interface. Even though the solubility of Ge is essentially the same in pure Hg and in Hg-In alloys, the local environment of each Ge nucleus for crystal growth during ec-LLS should differ strongly within these two liquid metals (Figures 5c,d). Specifically, In is a known 'surfactant' in vapor deposition of semiconductor films,[48,49] suggesting interfacial In will substantially affect Ge ec-LLS crystal growth.

The left panels of Figure 6 illustrate the resultant Ge crystal morphologies observed at a modest potential of -1.4 V vs *E*(Ag/AgCl) as a function of the In content in the Hg-In mixture. In pure Hg, Ge crystallites had a branched 'seaweed' structure indicative of fast crystal growth where the impinging zero-valent Ge atoms accumulated and remained at the site with the highest flux (i.e. the sharp tips). For liquid metals with increasing In content, the 'fine' detail of the leaf structure was lost and morphed into larger apparent grains. The right panels of Figure 6 suggest the origin of this morphology change. When In can accumulate at the crystal growth plane, surface transport of Ge adatoms to locales that minimize the overall free energy of the growing crystal surface is facilitated. In total, these data

indicated strongly that the liquid metal composition and structure could strongly influence the morphology of the product crystal.

With Hg-In alloys, we separately explored the possibility that the liquid metal could also influence the *composition* of the ec-LLS product. We previously established that pure liquid metal solvent/electrodes in ec-LLS could also act as reactants.[22,23] In this way, the product composition was necessarily dependent on the liquid metal identity. However, we posited that liquid metal alloys could further widen the synthetic fidelity if only one (or a subset) of components reacted with the electroreduced solute in ec-LLS.

For this purpose, we targeted the ec-LLS synthesis of In-Pd intermetallics.[50] Such compounds are interesting as selective hydrogenation catalysts.[51] Simply melting solid In and solid Pd together will produce a variety of different compositions and phases, depending on the temperature and relative proportions. At room temperature, the most stable intermetallic compound is In_7Pd_3. We were curious whether this same composition would be formed if Pd was electrodeposited into various liquid Hg-In alloys at a constant potential of -1.85 V vs. *E*(Ag/AgCl). Using $Pd(CN)_2$ as the oxidized precursor in an alkaline aqueous electrolyte, we performed ec-LLS using open, bulk liquid Hg-In pools (Figures 7a,b). X-ray diffraction data were collected for these materials and those collected for analogous experiments with solid In electrodes replacing the liquid metal electrodes. The diffraction signatures of all of these materials were compared to the most probable crystalline phases spanning pure Pd, Hg-Pd compounds, or In-Pd compounds (Figure 7c).

Several data features were notable. First, the product was not pure Pd, indicating chemical reaction between electrodeposited Pd and the electrode. Second, the material collected from solid In electrodes was exclusively In_7Pd_3, as predicted strictly based on thermodynamics. Third, the materials collected from the liquid Hg-In electrodes were *not* exclusively or predominantly In_7Pd_3. Rather, these products were consistent with the composition and crystal structure of InPd. The positions of the diffraction signals for the 110, 200, 211, and 220 crystallographic directions in InPd shifted to smaller 2θ values as the In content in the liquid metals increased (Figure 7d), consistent with distortion in the lattice parameter for InPd from Hg incorporation.

These facts indicated an ec-LLS process featuring metal exchange between the nascent nuclei/crystals and the liquid metal solvent (Figure 7e). We posited that Hg first reacts with the electrodeposited solute (Pd), rapidly forming an intermediate Hg-Pd phase. Electrodeposition of Pd using pure liquid Hg electrodes confirmed the existence of cubic HgPd but with low total mass yields,

presumably because HgPd had limited stability in contact with Hg. In Hg-In electrodes, site exchange between Hg and In stabilizes the solid and results in a In-Pd lattice with a similar (cubic) structure to Hg-Pd. The extent of the exchange between Hg and In at the lattice sites is a function of reaction rate, transport, and the activities of In and Hg in the liquid metal. In effect, InPd forms because HgPd is a reaction intermediate in this medium. Similar experiments performed with liquid Ga-In electrodes did not produce any InPd, further suggesting that HgPd was essential to the overall formation of InPd by ec-LLS under the employed conditions. Conversely, these experiments confirmed that Ga has a strong tendency to bind with the solute, providing a rationale for why Ga tends to incorporate heavily into crystallites produced by ec-LLS.

Outlook

The results and interpretations summarized here illustrate that ec-LLS remains fertile territory for both fundamental discovery and for applied technology development. As a platform for study, ec-LLS is well-suited for mechanistic studies to understand low temperature inorganic materials synthesis and crystallization because the set-up is simple and does not necessarily require elevated temperatures. Similarly, as a fabrication method, the ec-LLS concept could have value in the manufacture of technologies like photovoltaics and microelectronics if further control over the purity is realized. Using advanced analytical methods including in-situ TEM and XRR, we now know that nucleation and crystal growth in ec-LLS has both strong parallels and stark differences to more traditional melt crystal growth methods. More work is needed to develop predictive, quantitative models that describe the metallurgical chemistry of other low-melting point liquid metals at the extreme supersaturations in low temperature ec-LLS. We hope this account will spur such research.

Acknowledgements

Ms. Elizabeth Troia is recognized for assistance with figure preparation. J. H. acknowledges support from the NSF GRFP. S.M. thanks generous support from the National Science Foundation (#2106315) and the American Chemical Society Petroleum Research Fund (# 59671-ND10).

Biographies

Henry Wu received a B.S. in Biochemistry from Portland State University in 2019, performing research under Dr. Marilyn Mackiewicz on the toxicity of silver towards zebra fish. He joined the

University of Michigan as a doctoral student under the guidance of Prof. Maldonado and is presently working on preparing materials for electrocatalytic and electronic applications.

Joshua P. Hazelnis received a BA in Chemistry and BS in Chemical Engineering from the University at Buffalo in 2020, working alongside Prof. Timothy R. Cook on ion exchange membrane crossover in non-aqueous redox flow batteries. He joined the University of Michigan and is currently working on characterization of liquid metal/electrolyte interfaces.

Stephen Maldonado received a BS in Chemistry from the University of Iowa in 2001 and received his Ph.D. from the University of Texas at Austin in 2006 under Prof. Keith Stevenson. After two years at Caltech as a postdoctoral fellow with Prof. Nathan Lewis, he began his independent career at the University of Michigan. His research interests are developing electroanalytical methods in semiconductor electrochemistry and inventing electrosynthetic methods that enable 'green' pathways to valuable materials and chemicals.

Figures

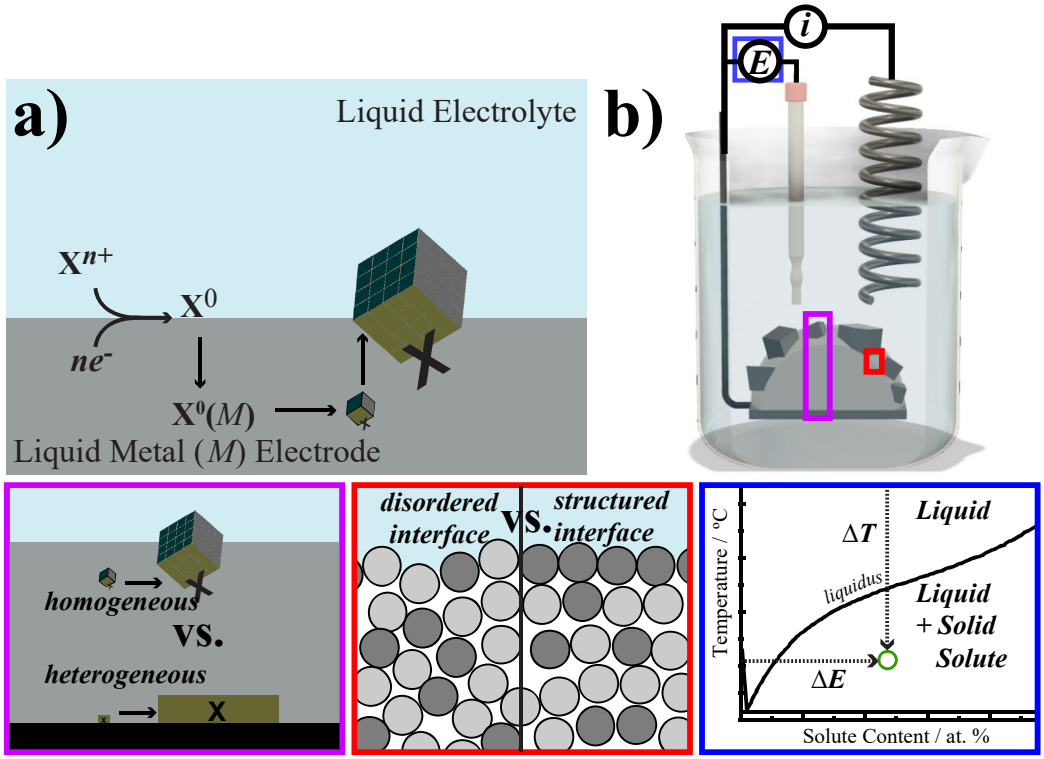

Figure 1. a) Schematic representation of ec-LLS. b) A three-electrode ec-LLS reaction cell with a liquid metal cathode. Colored boxed insets highlight three distinct topics: (purple) location of the nucleation/crystal growth events, (red) ordering of alloy atoms at the liquid metal interface, and (blue) electrochemical vs thermal pathways to reach supersaturation.

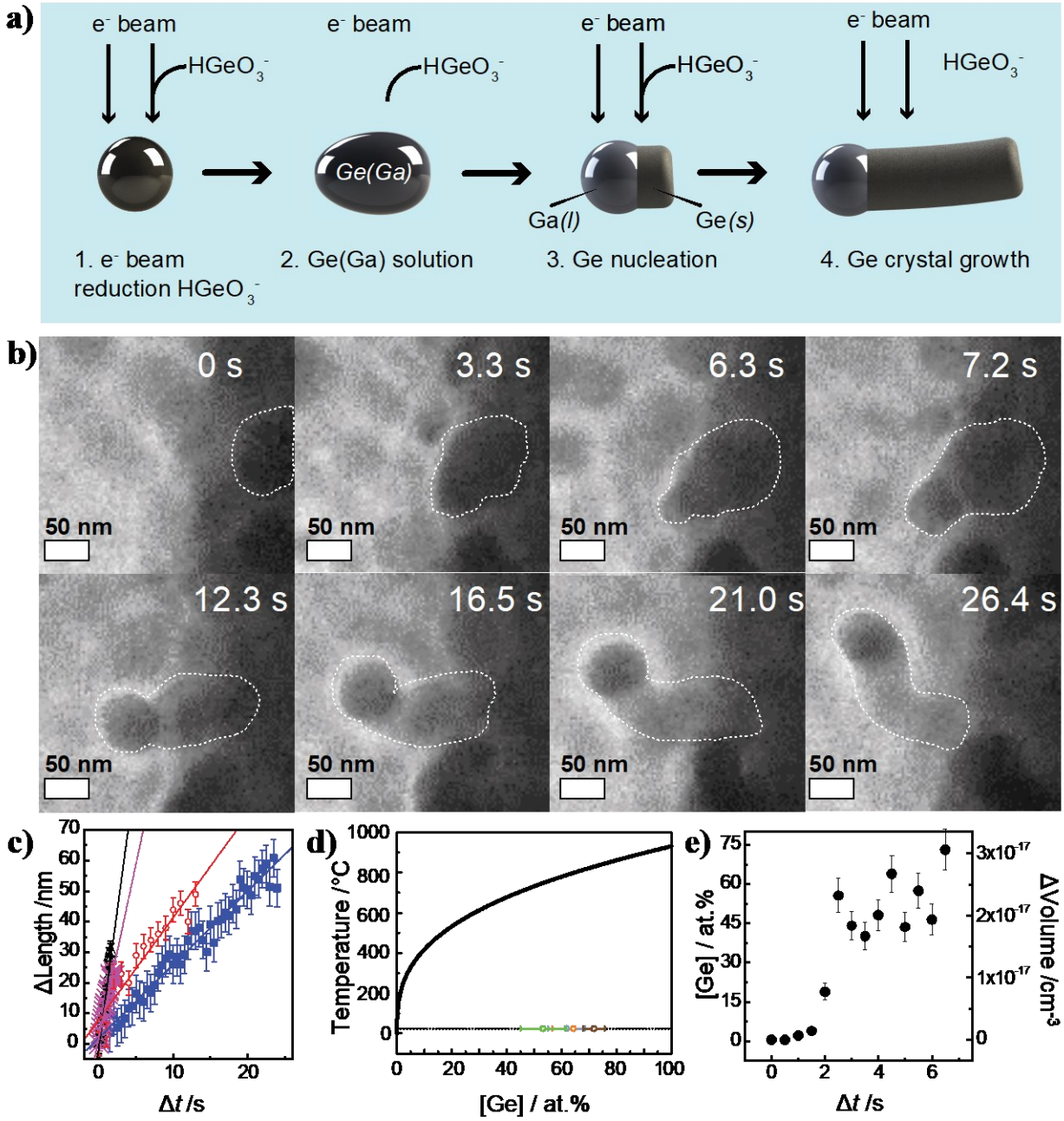

Figure 2. a) Schematic depiction of (*1*) an e⁻ beam causing the reduction of dissolved GeO_2 in solution to Ge^0, followed by (*2*) dissolution into the liquid metal, then (*3*) nucleation, and (*4*) Ge nanowire growth. b) Frame grabs from an *in situ* TEM video of a Ge ec-LLS event with a Ga nanodroplet immersed in an aqueous solution containing 0.05 M GeO_2 and 0.01 M $Na_2B_4O_7$. c) Nanowire length *vs* time for four separate Ge nanowire growth events. The steady-state growth rates were estimated from the linear-least-squares fitting of the data (red lines). d) The phase diagram for the Ga-Ge system with the inclusion of data from four different Ge nanowire growth events. The colored data points correspond to the inferred Ge concentration in the Ga nanodroplets at the time just before nucleation. e) Volume change of the Ga nanodroplet as a function of time before Ge nucleation occurred.

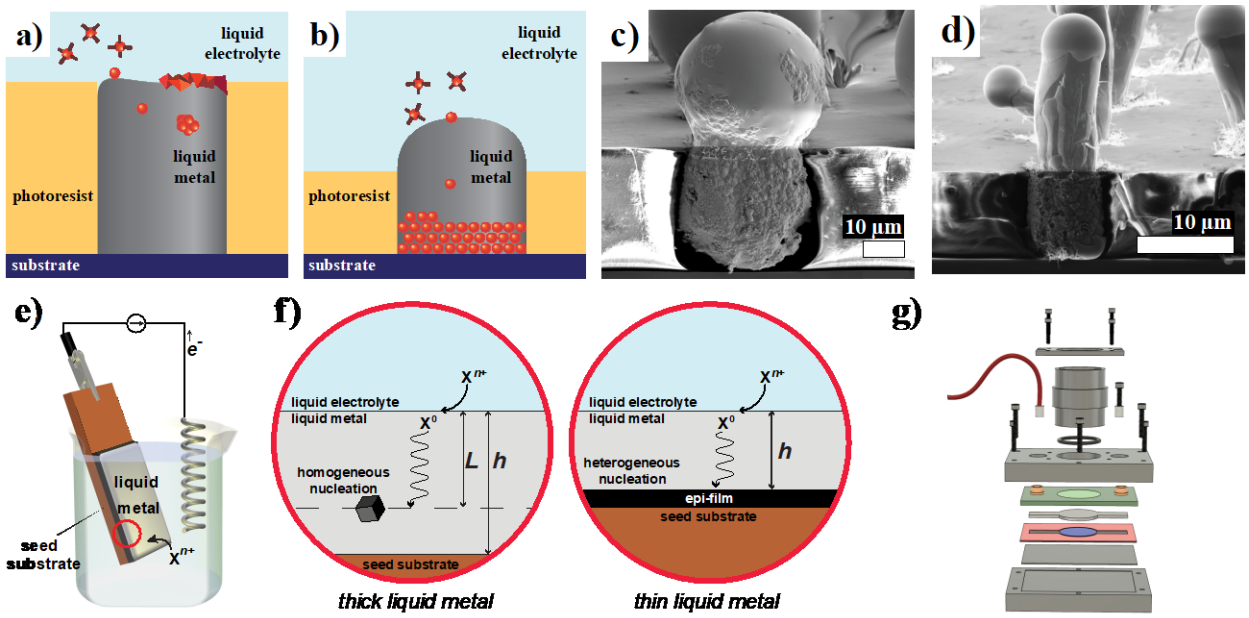

Figure 3. a) Schematic depiction of ec-LLS inside a microwell sufficiently deep that no solute reaches the bottom interface and instead preferentially nucleates and grows crystals homogeneously within the liquid metal. b) Same as in (a) except the microwell is so shallow that solutes preferentially nucleate heterogeneously. c,d) SEM images of Ge ec-LLS experiments performed in aqueous solution containing 50 mM GeO_2 and 10 mM $Na_2B_4O_7$ at $E = -1.6$ V for 30 min at $T = 40$°C using (c) 27 and (d) 8 µm thick *e*-GaIn. e) Summary view of an electrochemical liquid phase epitaxy film growth with a thin liquid metal electrode with thickness h that produces a black epifilm. f) A magnified view of area circled in red in (e) for two extreme cases. Left: A process where an electroreduced solute diffuses away from the liquid electrolyte/liquid metal interface before precipitating out in the liquid metal at some depth L. Right: A similar process except $h < L$, allowing for heterogeneous nucleation and crystal growth at the bottom interface. g) Exploded view of the ec-LPE cell that facilitates formation of a stable liquid metal film over a large two-dimensional area under bias.

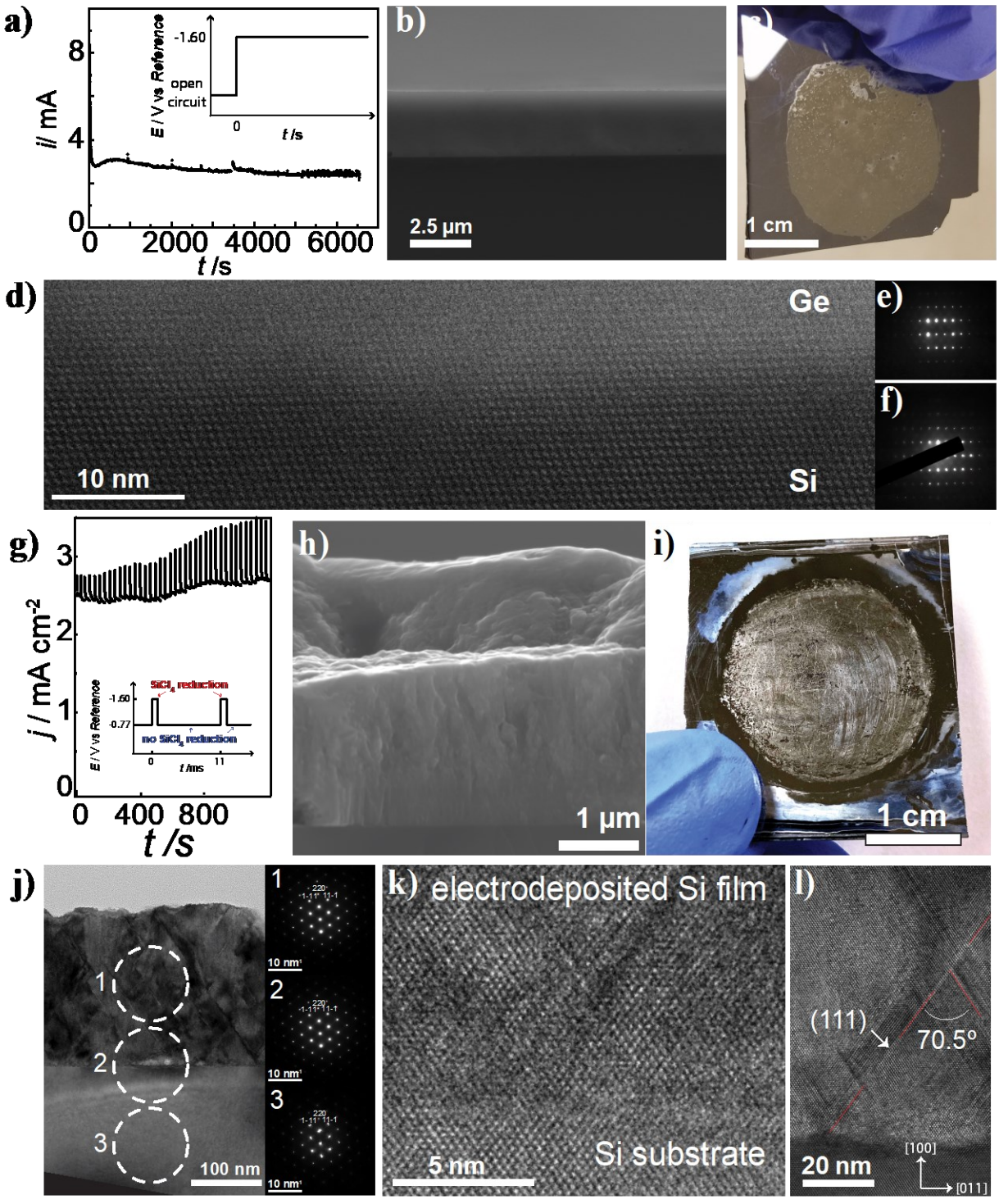

Figure 4. a) Representative chronoamperogram of a Ge film ec-LPE deposition at $E = -1.6$ V vs E(Ag/AgCl), $T = 90$ °C, and with an aqueous electrolyte containing 70 mM $Na_2B_4O_7$ and a formal concentration of 225 mM for GeO_2. b) Optical photograph of a Ge epifilm prepared with the same conditions as in (a). c) Cross-section SEM image Ge epifilms prepared with the same conditions as in (a). d) High resolution annular dark-field STEM image of the interface between the Ge film and Si

substrate. Electron diffraction patterns for the Ge film and the Ge/Si interface are shown in (e) and (f). g) Chronoamperogram for Si ec-LPE performed with *e*-GaIn liquid metal within an ec-LPE cell filled with propylene carbonate containing 0.1 M $(C_4H_9)_4NCl$ and 0.5 M $SiCl_4$ at T = 125°C. (Inset) Excitation waveform. h) Cross-section scanning electron micrograph of Si film grown by ec-LPE i) Plan view image of electrodeposited Si film prepared by ec-LPE at the conditions in (g). j) Bright field TEM cross section of a Si epifilm. Dashed circles: positions of the selected area aperture for the SAED in insets 1-3. k) High magnification bright field STEM of Si epifilm grown by ec-LPE. l) Representative high angle annular dark field high-resolution STEM of the interface between the Si film and substrate.

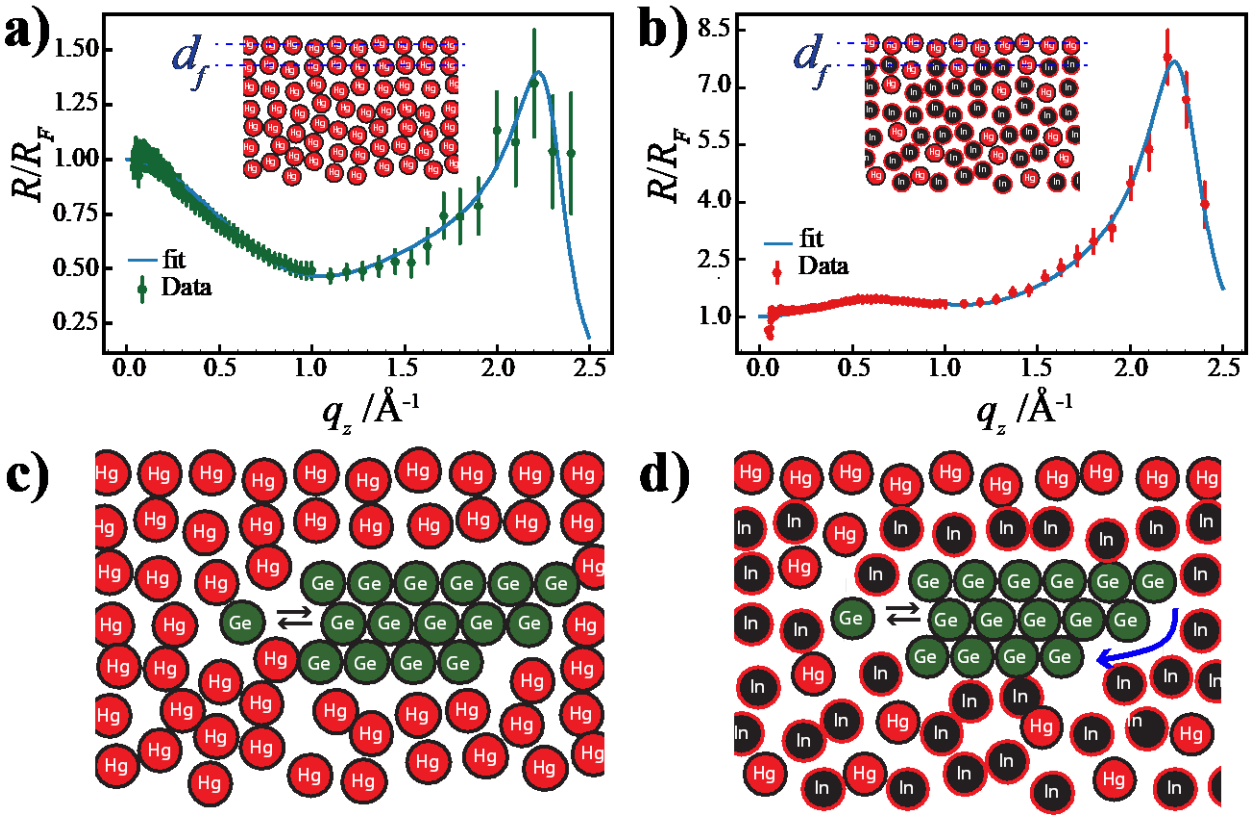

Figure 5. Normalized X-ray reflectivity of (a) liquid Hg and (b) liquid $Hg_{0.3}In_{0.7}$ in 0.1 M $Na_2B_4O_7$ at a potential of $E = -1.4$ V. The solid lines in (a, b) indicate the best fits. Insets: Schematic representations of the interface structure for each liquid metal. c,d) Schematic depiction of Ge crystal nucleus growth within (c) pure Hg and (d) Hg-In.

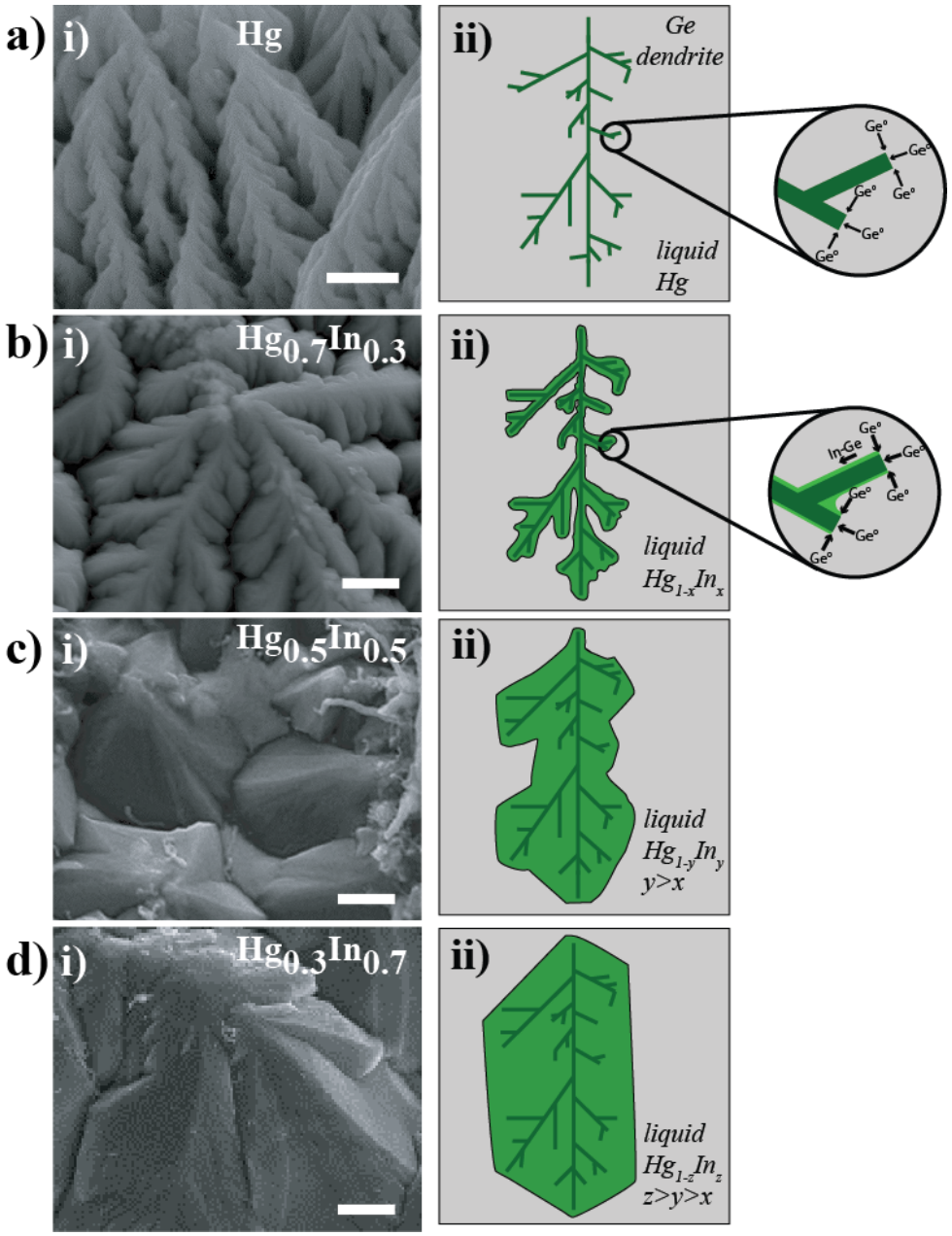

Figure 6. SEM images of as-prepared crystalline Ge electrodeposited with Hg, $Hg_{1-x}In_x$, and In electrodes from solutions containing 0.05 M GeO_2 and 0.01 M $Na_2B_4O_7$. Corresponding schematic depiction of the influence of Ge surface diffusion on morphology as a function of In concentration. Scale bars: (a) 0.5 μm; (b, c, d) 1 μm.

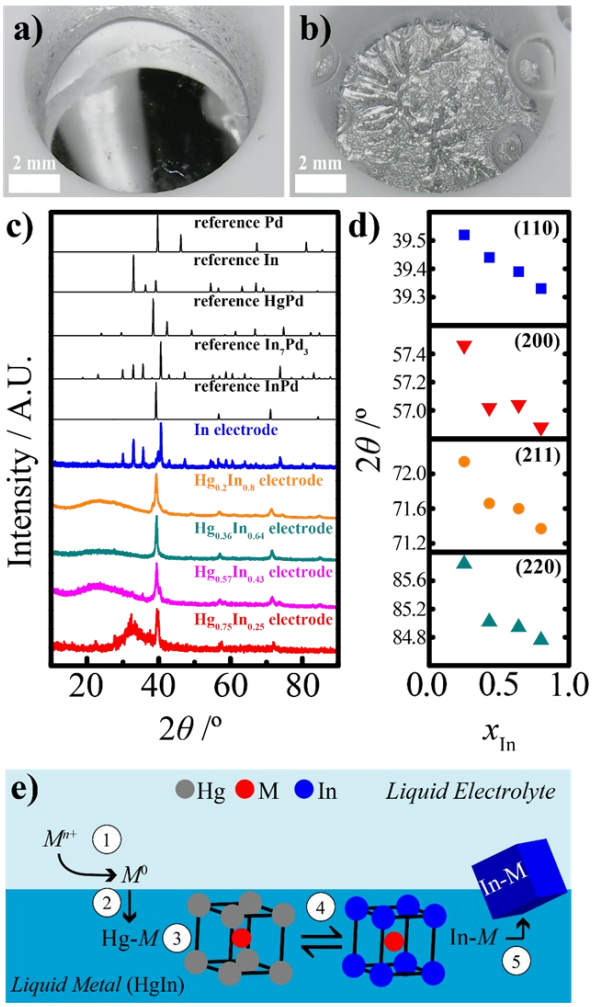

Figure 7. Photographs of Pd electrodeposited onto a Hg-In alloy electrode at a) $t = 0$ and b) 7900 s. c) Powder X-ray diffractograms collected after Pd electrodeposition with either liquid Hg-In or solid In electrodes. Reference peaks for polycrystalline Pd, In, HgPd, In_7Pd_3, and InPd. d) Shift in the peak position for the [100], [200], [211], and [220] InPd peaks as a function of the fraction of In in the Hg-In alloy used for material synthesis. e) Schematic depiction of the formation of In-*M* intermetallics by ec-LLS. Adapted with permission from ref. 50. Copyright 2022 The Electrochemical Society.

References.

(1) Cheek, Q.; Fahrenkrug, E.; Hlynchuk, S.; Alsem, D. H.; Salmon, N. J.; Maldonado, S. In Situ Transmission Electron Microscopy Measurements of Ge Nanowire Synthesis with Liquid Metal Nanodroplets in Water. *ACS Nano* **2020**, *14*, 2869-2879.

(2) Demuth, J.; Fahrenkrug, E.; Ma, L.; Shodiya, T.; Deitz, J. I.; Grassman, T. J.; Maldonado, S. Electrochemical Liquid Phase Epitaxy (ec-LPE): A New Methodology for the Synthesis of Crystalline Group IV Semiconductor Epifilms. *Journal of the American Chemical Society* **2017**, *139*, 6960-6968.

(3) Downes, N.; DeMuth, J.; Waelder, J.; Cheek, Q. B.; Bartels, H.; Maldonado, S. Si Electrochemical Liquid Phase Epitaxy: Low-Temperature Growth of Hyperdoped Epitaxial Si Films. *Chemistry of Materials* **2022**, *34*, 10861-10872.

(4) Pattadar, D.; Cheek, Q.; Sartori, A.; Zhao, Y.; Giri, R. P.; Murphy, B.; Magnussen, O.; Maldonado, S. Evidence for Facilitated Surface Transport during Ge Crystal Growth by Indium in Liquid Hg–In Alloys at Room Temperature. *Crystal Growth & Design* **2021**, *21*, 1645-1656.

(5) Czochralski, J. A new method for the measurement of the crystallization rate of metals. *Zeitschrift für physikalische Chemie* **1918**, *92*, 219-221.

(6) Mauk, M. G.: 6 - Liquid-Phase Epitaxy. In *Handbook of Crystal Growth (Second Edition)*; Kuech, T. F., Ed.; North-Holland: Boston, 2015; pp 225-316.

(7) Benbow, E. M.; Dalal, N. S.; Latturner, S. E. Crystal growth and magnetic behavior of R6T13−xAlxMy phases (R=La, Nd; T=Mn, Fe; M=main group) grown from lanthanide-rich eutectic fluxes. *Journal of Solid State Chemistry* **2009**, *182*, 3055-3062.

(8) He, H.; Tyson, C.; Saito, M.; Bobev, S. Synthesis and structural characterization of the ternary Zintl phases AE3Al2Pn4 and AE3Ga2Pn4 (AE=Ca, Sr, Ba, Eu; Pn=P, As). *Journal of Solid State Chemistry* **2012**, *188*, 59-65.

(9) Stojanovic, M.; Latturner, S. E. Growth of new ternary intermetallic phases from Ca/Zn eutectic flux. *Journal of Solid State Chemistry* **2007**, *180*, 907-914.

(10) Kanatzidis, M. G.; Pöttgen, R.; Jeitschko, W. The Metal Flux: A Preparative Tool for the Exploration of Intermetallic Compounds. *Angewandte Chemie International Edition* **2005**, *44*, 6996-7023.

(11) Sebastian, C. P.; Malliakas, C. D.; Chondroudi, M.; Schellenberg, I.; Rayaprol, S.; Hoffmann, R.-D.; Pöttgen, R.; Kanatzidis, M. G. Indium Flux-Growth of Eu2AuGe3: A New Germanide with an AlB2 Superstructure. *Inorganic Chemistry* **2010**, *49*, 9574-9580.

(12) Kalantar-Zadeh, K.; Rahim, M. A.; Tang, J. Low Melting Temperature Liquid Metals and Their Impacts on Physical Chemistry. *Accounts of Materials Research* **2021**, *2*, 577-580.

(13) Martin, A.; Du, C.; Chang, B.; Thuo, M. Complexity and Opportunities in Liquid Metal Surface Oxides. *Chemistry of Materials* **2020**, *32*, 9045-9055.

(14) Zavabeti, A.; Ou, J. Z.; Carey, B. J.; Syed, N.; Orrell-Trigg, R.; Mayes, E. L. H.; Xu, C.; Kavehei, O.; O'Mullane, A. P.; Kaner, R. B.; Kalantar-zadeh, K.; Daeneke, T. A liquid metal reaction environment for the room-temperature synthesis of atomically thin metal oxides. *Science* **2017**, *358*, 332.

(15) Dong, R.; Zhang, T.; Feng, X. Interface-Assisted Synthesis of 2D Materials: Trend and Challenges. *Chemical Reviews* **2018**, *118*, 6189-6235.

(16) Ghasemian, M. B.; Mayyas, M.; Idrus-Saidi, S. A.; Jamal, M. A.; Yang, J.; Mofarah, S. S.; Adabifiroozjaei, E.; Tang, J.; Syed, N.; O'Mullane, A. P.; Daeneke, T.; Kalantar-Zadeh, K. Self-Limiting Galvanic Growth of MnO2 Monolayers on a Liquid Metal—Applied to Photocatalysis. *Advanced Functional Materials* **2019**, *29*, 1901649.

(17) Elsen, A.; Festersen, S.; Runge, B.; Koops, C. T.; Ocko, B. M.; Deutsch, M.; Seeck, O. H.; Murphy, B. M.; Magnussen, O. M. In situ X-ray studies of adlayer-induced crystal nucleation at the liquid–liquid interface. *Proceedings of the National Academy of Sciences* **2013**, *110*, 6663.

(18) David, R.; Miki, N. Tunable Noble Metal Thin Films on Ga Alloys via Galvanic Replacement. *Langmuir* **2018**, *34*, 10550-10559.

(19) Wang, S.; Mao, Q.; Ren, H.; Wang, W.; Wang, Z.; Xu, Y.; Li, X.; Wang, L.; Wang, H. Liquid Metal Interfacial Growth and Exfoliation to Form Mesoporous Metallic Nanosheets for Alkaline Methanol Electroreforming. *ACS Nano* **2022**, *16*, 2978-2987.

(20) Kochat, V.; Samanta, A.; Zhang, Y.; Bhowmick, S.; Manimunda, P.; Asif Syed Asif, S.; Stender Anthony, S.; Vajtai, R.; Singh Abhishek, K.; Tiwary Chandra, S.; Ajayan Pulickel, M. Atomically thin gallium layers from solid-melt exfoliation. *Science Advances* **2018**, *4*, e1701373.

(21) Fahrenkrug, E.; Maldonado, S. Electrochemical Liquid–Liquid–Solid (ec-LLS) Crystal Growth: A Low-Temperature Strategy for Covalent Semiconductor Crystal Growth. *Accounts of Chemical Research* **2015**, *48*, 1881-1890.

(22) Fahrenkrug, E.; Gu, J.; Maldonado, S. Electrodeposition of Crystalline GaAs on Liquid Gallium Electrodes in Aqueous Electrolytes. *Journal of the American Chemical Society* **2013**, *135*, 330-339.

(23) DeMuth, J.; Ma, L.; Fahrenkrug, E.; Maldonado, S. Electrochemical Liquid-Liquid-Solid Deposition of Crystalline Gallium Antimonide. *Electrochimica Acta* **2016**, *197*, 353-361.

(24) DeMuth, J.; Ma, L.; Lancaster, M.; Acharya, S.; Cheek, Q.; Maldonado, S. Eutectic-Bismuth Indium as a Growth Solvent for the Electrochemical Liquid-Liquid-Solid Deposition of Germanium Microwires and Coiled Nanowires. *Crystal Growth & Design* **2018**, *18*, 677-685.

(25) Fahrenkrug, E.; Biehl, J.; Maldonado, S. Electrochemical Liquid–Liquid–Solid Crystal Growth of Germanium Microwires on Hard and Soft Conductive Substrates at Low Temperature in Aqueous Solution. *Chemistry of Materials* **2015**, *27*, 3389-3396.

(26) Zhao, Z.; Yang, C.; Wu, L.; Zhang, C.; Wang, R.; Ma, E. Preparation and Characterization of Crystalline Silicon by Electrochemical Liquid–Liquid–Solid Crystal Growth in Ionic Liquid. *ACS Omega* **2021**, *6*, 11935-11942.

(27) Ma, L.; Lee, S.; DeMuth, J.; Maldonado, S. Direct electrochemical deposition of crystalline silicon nanowires at T≥ 60° C. *RSC Advances* **2016**, *6*, 78818-78825.

(28) Acharya, S.; Ma, L.; Maldonado, S. Critical Factors in the Growth of Hyperdoped Germanium Microwires by Electrochemical Liquid–Liquid–Solid Method. *ACS Applied Nano Materials* **2018**, *1*, 5553-5561.

(29) Pershan, P. S.; Schlossman, M.: *Liquid Surfaces and Interfacs: Synchrotron X-ray Methods.*; Cambridge University Press: Cambridge, 2012.

(30) Regan, M. J.; Pershan, P. S.; Magnussen, O. M.; Ocko, B. M.; Deutsch, M.; Berman, L. E. X-ray reflectivity studies of liquid metal and alloy surfaces. *Physical Review B* **1997**, *55*, 15874-15884.

(31) Carim, A. I.; Collins, S. M.; Foley, J. M.; Maldonado, S. Benchtop Electrochemical Liquid–Liquid–Solid Growth of Nanostructured Crystalline Germanium. *Journal of the American Chemical Society* **2011**, *133*, 13292-13295.

(32) Ma, L.; Gu, J.; Fahrenkrug, E.; Maldonado, S. Electrochemical Liquid-Liquid-Solid Deposition of Crystalline Ge Nanowires as a Function of Ga Nanodroplet Size. *Journal of The Electrochemical Society* **2014**, *161*, D3044-D3050.

(33) Fahrenkrug, E.; Gu, J.; Jeon, S.; Veneman, P. A.; Goldman, R. S.; Maldonado, S. Room-Temperature Epitaxial Electrodeposition of Single-Crystalline Germanium Nanowires at the Wafer Scale from an Aqueous Solution. *Nano Letters* **2014**, *14*, 847-852.

(34) DeMuth, J.; Fahrenkrug, E.; Maldonado, S. Controlling Nucleation and Crystal Growth of Ge in a Liquid Metal Solvent. *Crystal Growth & Design* **2016**, *16*, 7130-7138.

(35) Biswas, S.; O'Regan, C.; Petkov, N.; Morris, M. A.; Holmes, J. D. Manipulating the Growth Kinetics of Vapor–Liquid–Solid Propagated Ge Nanowires. *Nano Letters* **2013**, *13*, 4044-4052.

(36) Kim, B. J.; Wen, C. Y.; Tersoff, J.; Reuter, M. C.; Stach, E. A.; Ross, F. M. Growth Pathways in Ultralow Temperature Ge Nucleation from Au. *Nano Letters* **2012**, *12*, 5867-5872.

(37) Schwalbach, E. J.; Voorhees, P. W. Phase Equilibrium and Nucleation in VLS-Grown Nanowires. *Nano Letters* **2008**, *8*, 3739-3745.

(38) Ross, F. M. Opportunities and challenges in liquid cell electron microscopy. *Science* **2015**, *350*, aaa9886.

(39) Han, C.; Islam, M. T.; Ni, C. In Situ TEM of Electrochemical Incidents: Effects of Biasing and Electron Beam on Electrochemistry. *ACS Omega* **2021**, *6*, 6537-6546.

(40) Liu, N.; Zhou, G.; Yang, A.; Yu, X.; Shi, F.; Sun, J.; Zhang, J.; Liu, B.; Wu, C.-L.; Tao, X.; Sun, Y.; Cui, Y.; Chu, S. Direct electrochemical generation of supercooled sulfur microdroplets well below their melting temperature. *Proceedings of the National Academy of Sciences* **2019**, *116*, 765-770.

(41) Grahame, D. C. The Electrical Double Layer and the Theory of Electrocapillarity. *Chemical Reviews* **1947**, *41*, 441-501.

(42) Maldonado, S. The Importance of New "Sand-to-Silicon" Processes for the Rapid Future Increase of Photovoltaics. *ACS Energy Letters* **2020**, *5*, 3628-3632.

(43) Gu, J.; Fahrenkrug, E.; Maldonado, S. Direct Electrodeposition of Crystalline Silicon at Low Temperatures. *Journal of the American Chemical Society* **2013**, *135*, 1684-1687.

(44) Downes, N.; Cheek, Q.; Maldonado, S. Electroreduction of Perchlorinated Silanes for Si Electrodeposition. *Journal of The Electrochemical Society* **2021**, *168*, 022503.

(45) Hazelnis, J. P.; Sartori, A.; Cheek, Q. B.; Giri, R. P.; MacInnes, M. M.; Murphy, B. M.; Magnussen, O. M.; Maldonado, S. Detection of Ge-Containing Adlayers at the Liquid Hg/Water Interface by In Situ X-ray Reflectivity in Aqueous Borate Electrolytes Containing Dissolved GeO2. *The Journal of Physical Chemistry C* **2022**, *126*, 8177-8189.

(46) Dumke, M. F.; Tombrello, T. A.; Weller, R. A.; Housley, R. M.; Cirlin, E. H. Sputtering of the gallium-indium eutectic alloy in the liquid phase. *Surface Science* **1983**, *124*, 407-422.

(47) Maruyama, T.; Matsuda, K.; Naritsuka, S. Multinuclear layer-by-layer growth on Ge(111) by LPE. *Journal of Crystal Growth* **2005**, *275*, e2155-e2160.

(48) Won, D.; Weng, X.; Redwing, J. M. Effect of indium surfactant on stress relaxation by V-defect formation in GaN epilayers grown by metalorganic chemical vapor deposition. *J. Appl. Phys.* **2010**, *108*, 093511.

(49) Won, D.; Weng, X.; Redwing, J. M. Metalorganic chemical vapor deposition of N-polar GaN films on vicinal SiC substrates using indium surfactants. *Appl. Phys. Lett.* **2012**, *100*, 021913.

(50) Wu, H.; Maldonado, S. Electrodeposition of Pd Intermetallics using Hg-In by the Electrochemical Liquid-Liquid-Solid Method. *Journal of The Electrochemical Society* **2022**, *169*, 112514.

(51) Yang, Y.; Wei, M. Intermetallic compound catalysts: synthetic scheme, structure characterization and catalytic application. *Journal of Materials Chemistry A* **2020**, *8*, 2207-2221.